

**Supplementary Information:**

**High-density, Ultraflexible Organic Electrochemical Transistor  
Array for Brain Activity Mapping**

Wei Xu,<sup>‡a</sup> Yanlan Zhu,<sup>‡a</sup> Xiaolin Zhou,<sup>‡b</sup> Haoyue Guo,<sup>b</sup> Jingxin Wang,<sup>a</sup> Ruiqi Zhu,<sup>a</sup> Zhengwei Hu,<sup>b</sup> Wei Ma,<sup>c</sup> Xing Ma,<sup>d</sup> Xiaojian Li,<sup>b</sup> and Xiaomin Xu<sup>a\*</sup>

<sup>a</sup>Institute of Materials Research, Tsinghua Shenzhen International Graduate School,  
Tsinghua University, Shenzhen 518055, China

<sup>b</sup>Centre for Brain Connectome and Behavior, The Brain Cognition and Brain Disease  
Institute of Shenzhen Institute of Advanced Technology, Shenzhen 518055, China

<sup>c</sup>State Key Laboratory for Mechanical Behavior of Materials,  
Xi'an Jiaotong University, Xi'an 710000, China

<sup>d</sup>School of Materials Science and Engineering, and Sauvage Laboratory for Smart  
Materials, Harbin Institute of Technology (Shenzhen), Shenzhen, Guangdong, 518055  
China

\*Correspondence should be sent to: [xu.xiaomin@sz.tsinghua.edu.cn](mailto:xu.xiaomin@sz.tsinghua.edu.cn)

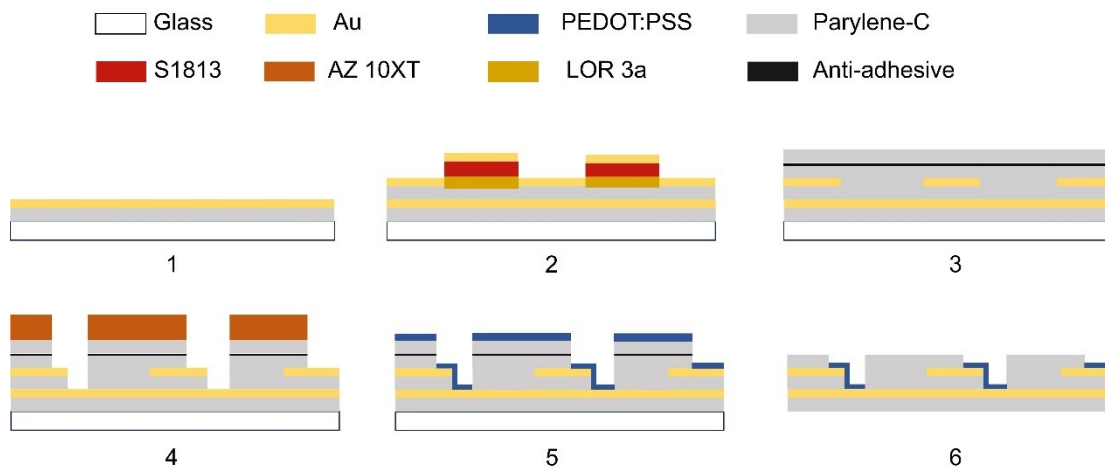


**Figure S1. Optical lithography-based microfabrication process of the vOECT array.** (1) Deposition of the first layer gold as source electrodes via photolithography and lift-off process. (2) Deposition of the intermediate insulating parylene-C layer and patterning of the second metal layer as drain electrodes. (3) Deposition of the encapsulation and sacrificial parylene-C layers. (4) Reactive ion etching step with photoresist etch mask to define channel. (5) Deposition of PEDOT:PSS using spin coating. (6) Peel-off of the sacrificial parylene-C layer.

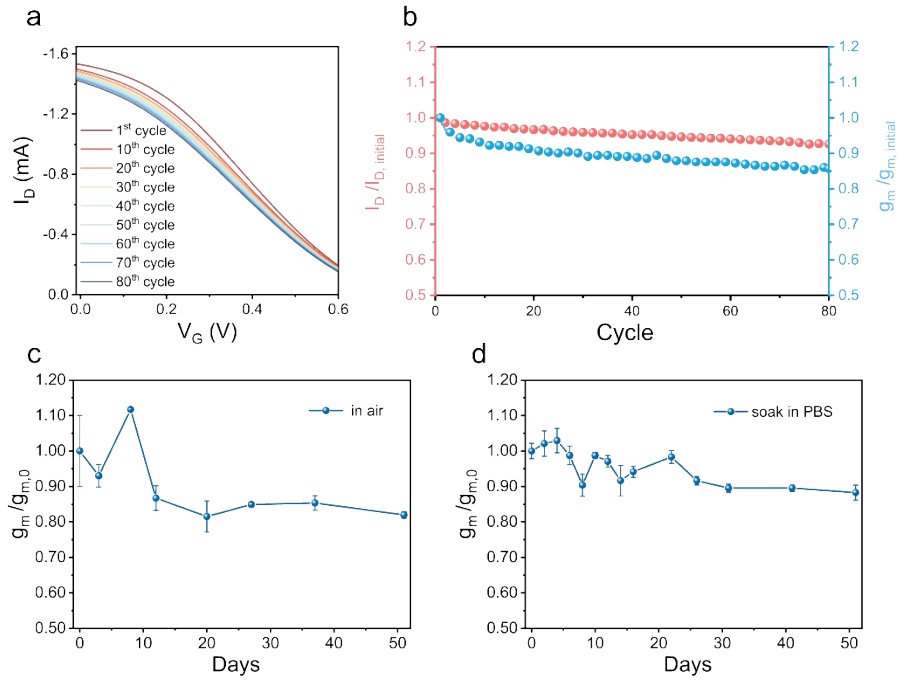


**Figure S2. Long-term recording stability.** a) Transfer curves throughout 80 consecutive cycles. b) The variations of on-state drain current and peak transconductance with the number of test cycles. The change in peak transconductance of the device over time when stored c) in air and d) in PBS. The error bars were calculated by computing the standard deviation of four OECTs within one sample.

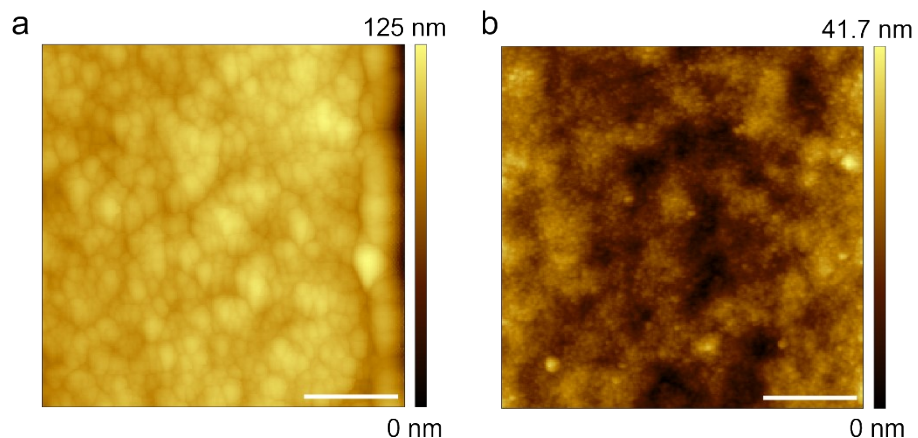


**Figure S3.** Atomic force microscopic (AFM) images of PEDOT:PSS films stored in air (a) and in phosphate buffered saline (PBS) solution (b), for 15 days. Scale bar: 1  $\mu\text{m}$ .

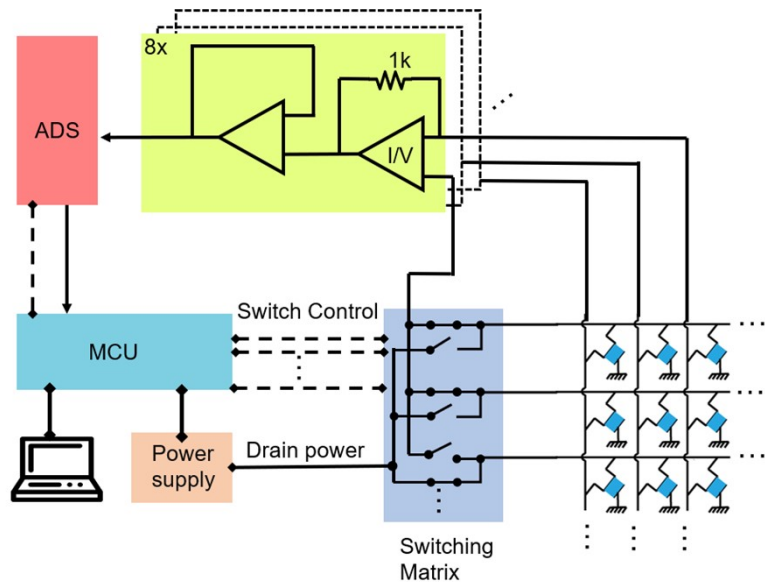


**Figure S4. Schematic of discrete multiplexing setup.**

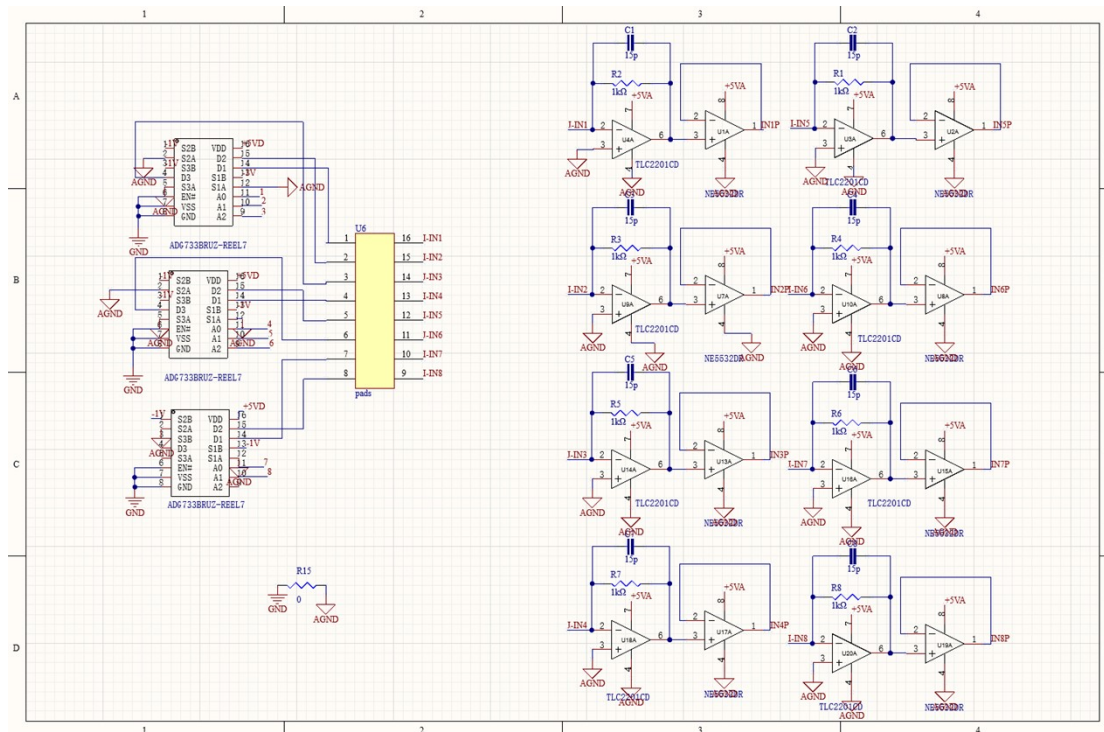


**Figure S5. Complete schematic of the data acquisition interface circuit board.**

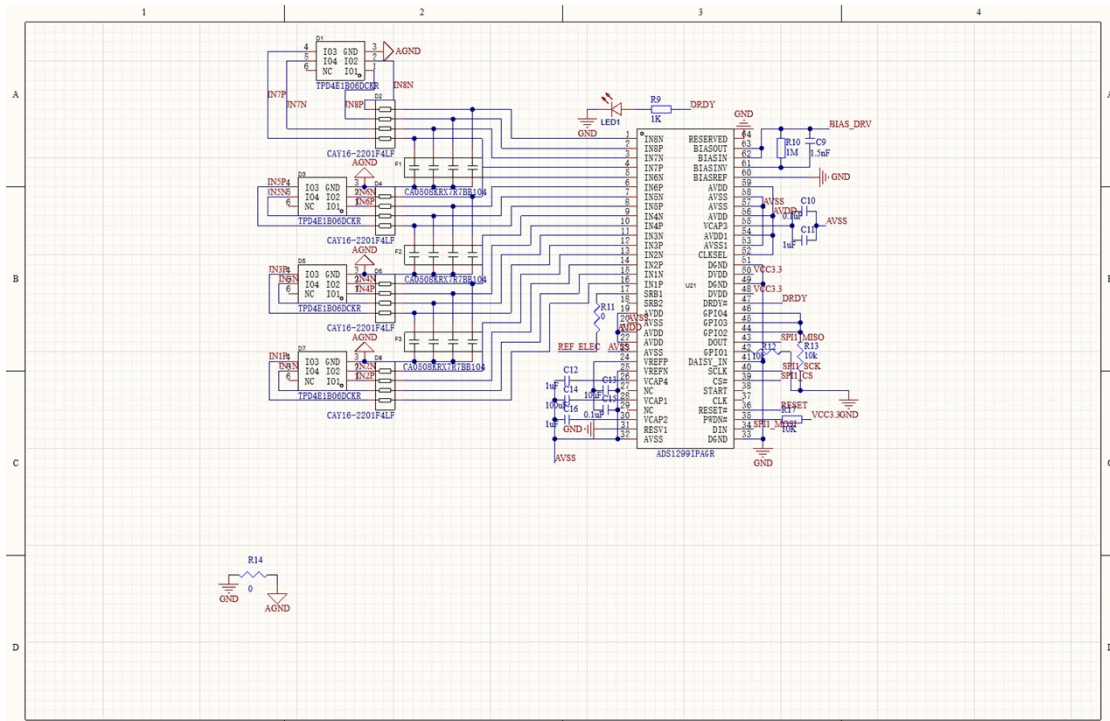


**Figure S6. Complete schematic of the data acquisition interface circuit board.**

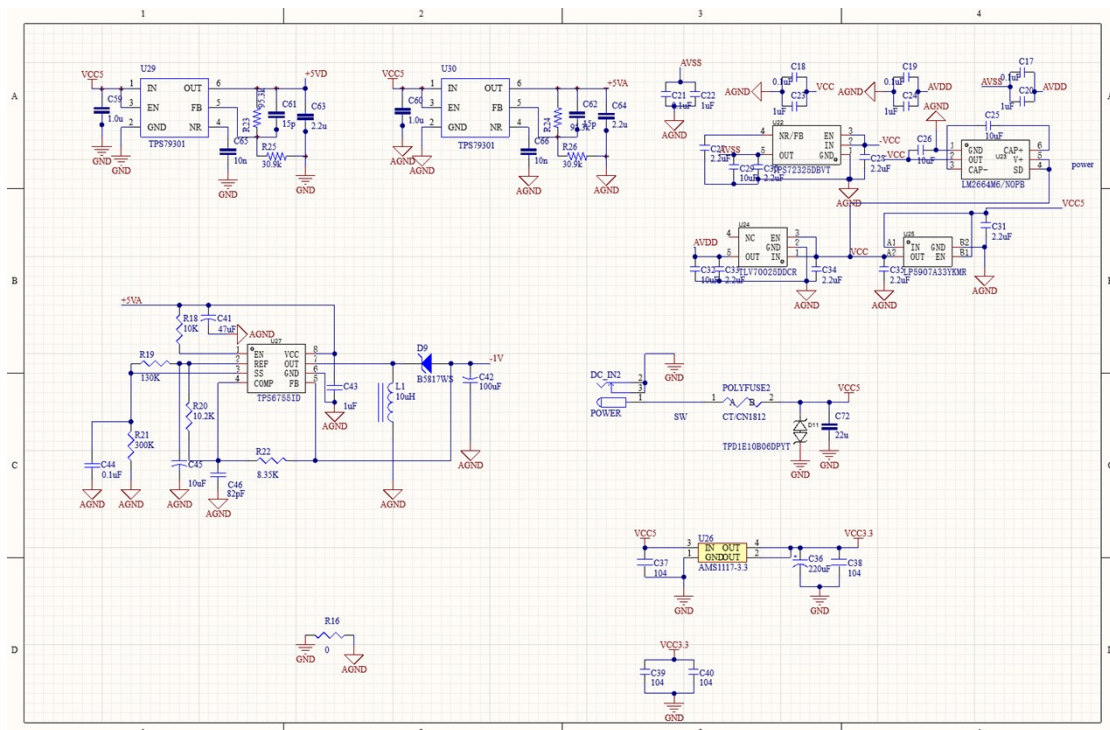


**Figure S7. Complete schematics of the data acquisition interface circuit board.**

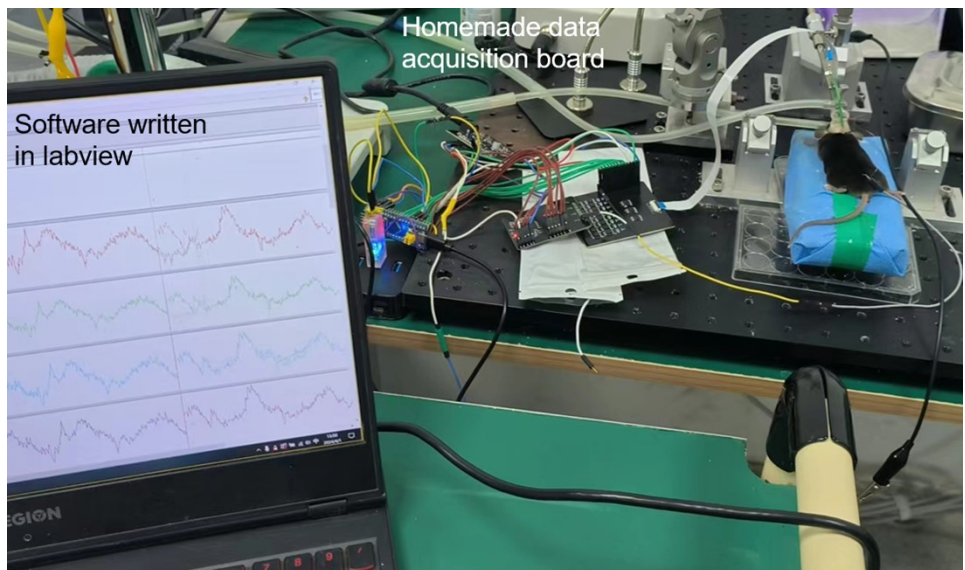


**Figure S8. Photograph of the home-built multiplexing acquisition system.**

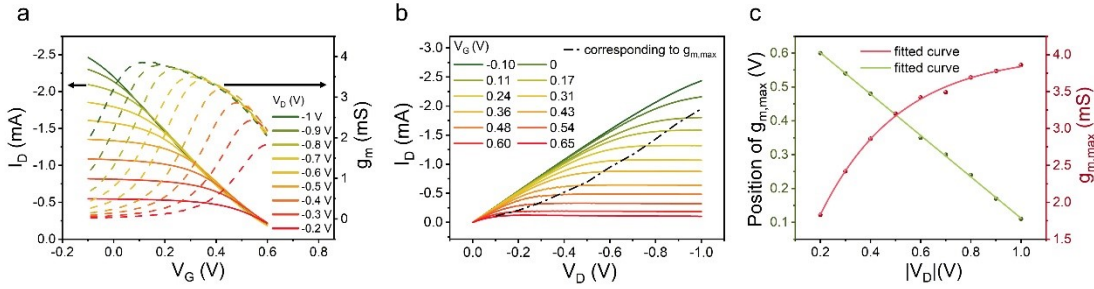


**Figure S9. The impact of drain voltage on device performance.** (a) Transfer curves, along with the  $g_m$  of the vOECT with a channel length ( $L$ ) of 0.6  $\mu\text{m}$ , channel width ( $W$ ) of 50  $\mu\text{m}$ , and a PEDOT:PSS thickness of 143 nm, under various drain biases. (b) Output curve depicting the variation of drain current with gate voltage ranging from  $-0.1$  V to  $0.65$  V. The dark dashed line marks the gate voltages  $V_G$  that correspond to  $g_{m,\max}$ . (c) The linear relationship between  $V_{g_{m,\max}}$  and  $|V_D|$ , and the asymptotic exponential relationship between  $g_{m,\max}$  and  $|V_D|$ .

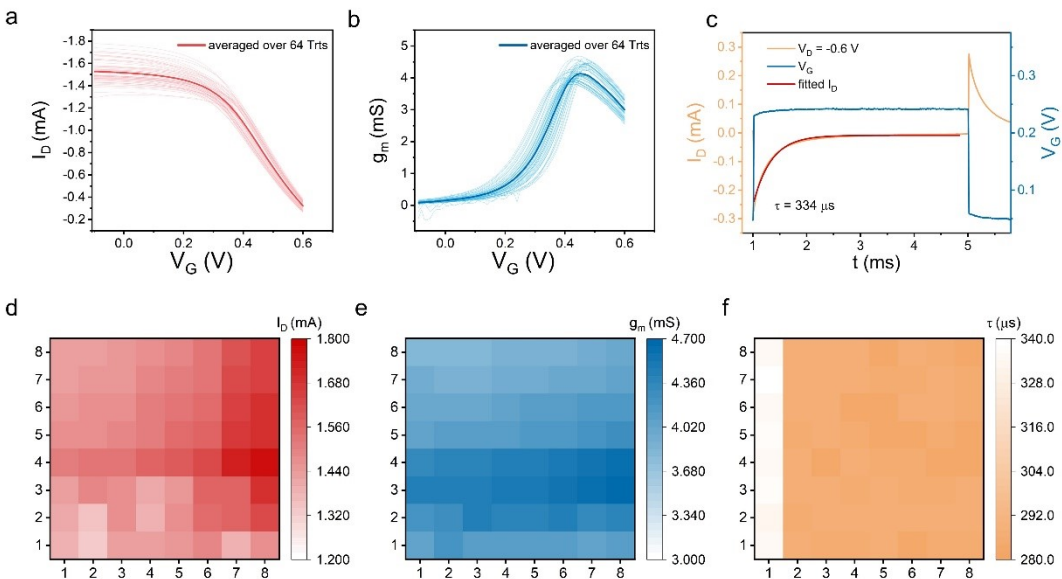


**Figure S10. Assessment of electrical performance homogeneity of an ultraflexible 64-channel array.** (a) Transfer characteristics of 64 vOECTs, showing drain current as a function of gate voltage. (b) Transconductance ( $g_m$ ) profiles corresponding to each device in the 64-channel array, demonstrating performance homogeneity. (c) Transient performance profile of a representative vOECT among the ultraflexible array, exhibiting a response time ( $\tau$ ) of 334  $\mu\text{s}$ . (d-f) Spatial distribution of  $I_D$  under zero gate bias (d), the peak  $g_m$  (e), and the response time  $\tau$  (f).

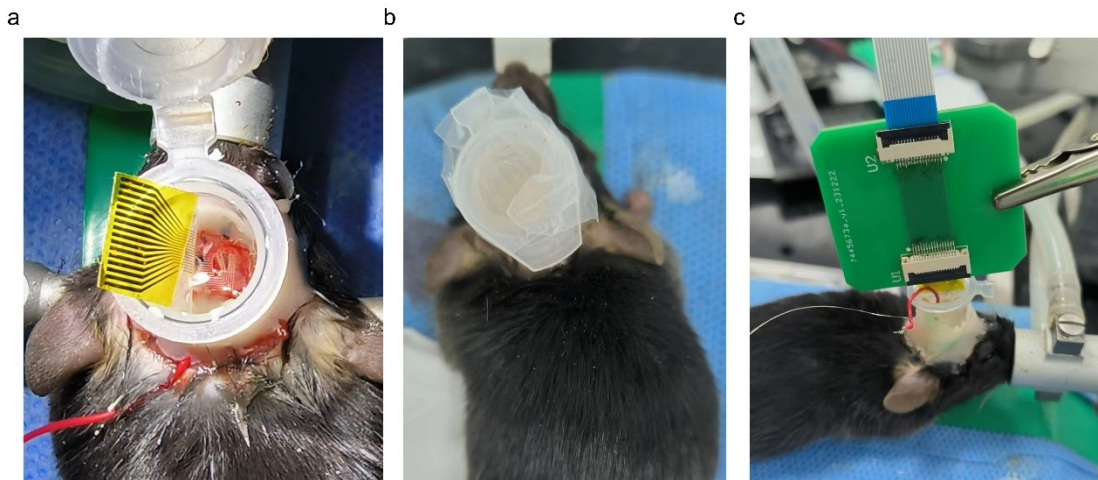


**Figure S11. Photograph of long-term implanted signal acquisition.** (a) Photograph of the vOECT array attached to the cerebral cortex and placed inside a cap made from a centrifuge tube. (b) Photograph showing the array stored inside the cap and sealed with parafilm. (c) Photograph showing the recording setup, where the cap is opened to connect the array to an adapter board using a ZIF connector.

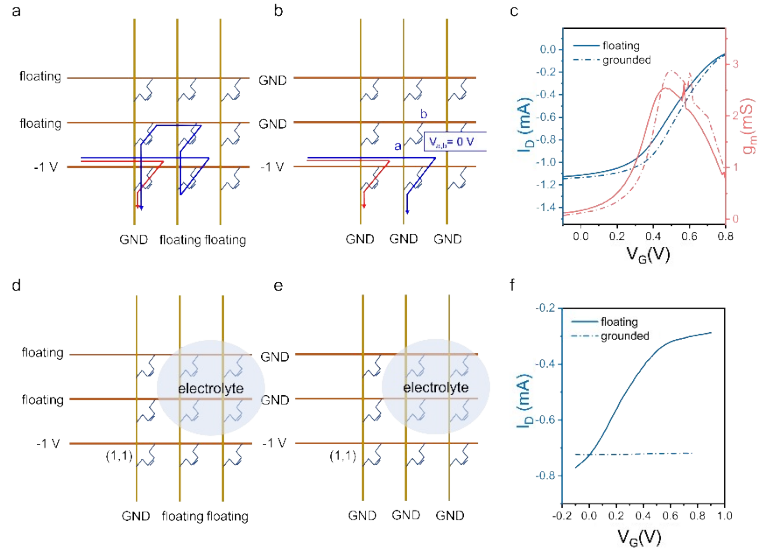


**Figure S12. Crosstalk evaluation.** (a) Illustration of the sources of crosstalk when the leads are floating. (b) Principle of crosstalk reduction achieved by grounding the floating sites ( $V_{a,b}=0$ ). (c) Comparison of transfer curves under floating and grounded conditions. (d, e) Crosstalk evaluation by measuring uncovered sites with (d) floating leads and (e) grounded leads. (f) Change in  $I_d$  of the (1,1) site following the application of gate voltage ( $V_g$ ) to the droplet.

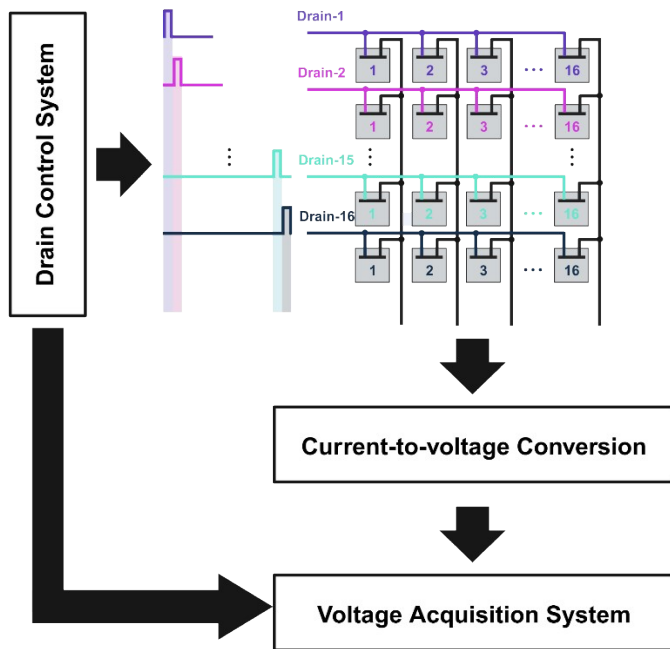


**Figure S13.** Schematic of the PXI setup.

**Table S1.** Performance comparison of the ultraflexible OECT array developed in this study with previously documented transistor arrays for electrophysiology.

	Number of Electrodes	Sensing area ( $\mu\text{m}^2$ )	Spacing ( $\mu\text{m}$ )	Density (sites/ $\text{mm}^2$ )	Response time ( $\mu\text{s}$ )	$g_m$ (mS)	Ref.
OECT	15	20 $\times$ 70	1000	1.00	363	1.1	1
	16	15 $\times$ 10	3000	0.11	60	3.5	2
	16	5 $\times$ 5	2000	0.25	62	2	3
	16	40 $\times$ 30	200	25	/	2.5	4
	25	8 $\times$ 32	4000	0.06	330	1.5	5
	64	30 $\times$ 20	200	25	291.3	4.19	This work
	100	200 $\times$ 20	870	1.56	1,420	8.67	6
	1024	30 $\times$ 20	100	100	233	2.07	This work
G-sgfet	32	50 $\times$ 50	400	6.25	909	1.2	7
	64	50 $\times$ 50	400	6.25	10,000	1.8	8
Si-based arrays	360	500 $\times$ 500	500	4.00	/	/	9
	1008	100 $\times$ 180	250	12.12	/	/	10
	1152	50 $\times$ 50	295	11.5	/	/	11

Note: G-sgfet represents graphene solution-gated field effect transistor.

## References

1. W. Lee, D. Kim, N. Matsuhisa, M. Nagase, M. Sekino, G. G. Malliaras, T. Yokota and T. Someya, *Proc. Natl. Acad. Sci. U.S.A.*, 2017, **114**, 10554-10559.
2. W. Lee, S. Kobayashi, M. Nagase, Y. Jimbo, I. Saito, Y. Inoue, T. Yambe, M. Sekino, G. G. Malliaras, T. Yokota, M. Tanaka and T. Someya, *Sci. Adv.*, 2018, **4**, eaau2426.
3. Y. Jimbo, D. Sasaki, T. Ohya, S. Lee, W. Lee, F. Arab Hassani, T. Yokota, K. Matsuura, S. Umezu, T. Shimizu and T. Someya, *Proc. Natl. Acad. Sci. U.S.A.*, 2021, **118**, e2022300118.
4. X. Gu, C. Yao, Y. Liu and I.-M. Hsing, *Adv. Healthcare Mater.*, 2016, **5**, 2345-2351.
5. W. Lee, D. Kim, J. Rivnay, N. Matsuhisa, T. Lonjaret, T. Yokota, H. Yawo, M. Sekino, G. G. Malliaras and T. Someya, *Adv. Mater.*, 2016, **28**, 9722-9728.
6. M. Wu, K. Yao, N. Huang, H. Li, J. Zhou, R. Shi, J. Li, X. Huang, J. Li, H. Jia, Z. Gao, T. H. Wong, D. Li, S. Hou, Y. Liu, S. Zhang, E. Song, J. Yu and X. Yu, *Adv. Sci.*, 2023, **10**, 2300504.
7. R. Garcia-Cortadella, N. Schäfer, J. Cisneros-Fernandez, L. Ré, X. Illa, G. Schwesig, A. Moya, S. Santiago, G. Guirado, R. Villa, A. Sirota, F. Serra-Graells, J. A. Garrido and A. Guimerà-Brunet, *Nano Lett.*, 2020, **20**, 3528-3537.
8. R. Garcia-Cortadella, G. Schwesig, C. Jeschke, X. Illa, A. L. Gray, S. Savage, E. Stamatidou, I. Schiessl, E. Masvidal-Codina, K. Kostarelos, A. Guimerà-Brunet, A. Sirota and J. A. Garrido, *Nat. Commun.*, 2021, **12**, 211.
9. J. Viventi, D.-H. Kim, L. Vigeland, E. S. Frechette, J. A. Blanco, Y.-S. Kim, A. E. Avrin, V. R. Tiruvadi, S.-W. Hwang, A. C. Vanleer, D. F. Wulsin, K. Davis, C. E. Gelber, L. Palmer, J. Van der Spiegel, J. Wu, J. Xiao, Y. Huang, D. Contreras, J. A. Rogers and B. Litt, *Nat. Neurosci.*, 2011, **14**, 1599-1605.
10. C.-H. Chiang, S. M. Won, A. L. Orsborn, K. J. Yu, M. Trumpis, B. Bent, C. Wang, Y. Xue, S. Min, V. Woods, C. Yu, B. H. Kim, S. B. Kim, R. Huq, J. Li, K. J. Seo, F. Vitale, A. Richardson, H. Fang, Y. Huang, K. Shepard, B. Pesaran, J. A. Rogers and J. Viventi, *Sci. Transl. Med.*, 2020, **12**, eaay4682.
11. T. Kaiju, M. Inoue, M. Hirata and T. Suzuki, *J. Neural Eng.*, 2021, **18**, 036025.